

# Absence of a Spin Liquid Phase in the Hubbard Model on the Honeycomb Lattice

Sandro Sorella<sup>1,2,3,\*</sup>, Yuichi Otsuka<sup>3,†</sup> and Seiji Yunoki<sup>3,4,5‡</sup>

<sup>1</sup>*SISSA – International School for Advanced Studies, Via Bonomea 265, 34136 Trieste, Italy,*

<sup>2</sup>*Democritos Simulation Center, CNR – IOM Istituto Officina dei Materiali, 34151 Trieste, Italy,*

<sup>3</sup>*Computational Materials Science Research Team, RIKEN AICS, Kobe, Hyogo 650-0047, Japan,*

<sup>4</sup>*Computational Condensed Matter Physics Laboratory, RIKEN ASI, Saitama 351-0198, Japan, and*

<sup>5</sup>*CREST, Japan Science and Technology (JST), Kawaguchi, Saitama 332-0012, Japan*

(Dated: May 13, 2018)

A spin liquid is a novel quantum state of matter with no conventional order parameter where a finite charge gap exists even though the band theory would predict metallic behavior. Finding a stable spin liquid in two or higher spatial dimensions is one of the most challenging and debated issues in condensed matter physics. Very recently, it has been reported that a model of graphene, i.e., the Hubbard model on the honeycomb lattice, can show a spin liquid ground state in a wide region of the phase diagram, between a semi-metal (SM) and an antiferromagnetic insulator (AFMI). Here, by performing numerically exact quantum Monte Carlo simulations, we extend the previous study to much larger clusters (containing up to 2592 sites), and find, if any, a very weak evidence of this spin liquid region. Instead, our calculations strongly indicate a direct and continuous quantum phase transition between SM and AFMI.

## Introduction

A spin liquid can be considered as a Mott insulator that is not adiabatically connected to any band insulator and does not break any symmetry even at zero temperature. Recently, much attention has been focused on a possible spin liquid in two or three spatial dimensions [1–5]. On one hand, it has been suggested experimentally that several organic materials represent good candidates for spin liquids [6–8]. On the other hand, the existence of a spin liquid has so far been demonstrated only in very few and particularly simplified models [9, 10].

In order to understand this issue, let us consider a model Hamiltonian on a lattice describing the insulating state of electrons at half-filling, i.e., one electron per lattice site. Since the charge gap is assumed, only spin degrees of freedom remain and can be described by the spin-1/2 Heisenberg model. Since any spin-1/2 model corresponds to a well defined interacting hard core boson model, the crucial question is to understand how – at zero temperature – these bosonic degrees of freedom can avoid Bose-Einstein condensation and/or crystallization, necessary conditions for a stable spin liquid with no long-range order of any kind.

In this report, we study the ground state of the half-filled Hubbard model on the honeycomb lattice (see Fig. 1) defined by the following Hamiltonian,

$$\hat{H} = -t \sum_{\langle i,j \rangle, \sigma} \left( c_{i\sigma}^\dagger c_{j\sigma} + c_{j\sigma}^\dagger c_{i\sigma} \right) + U \sum_i n_{i\uparrow} n_{i\downarrow}, \quad (1)$$

where  $c_{i\sigma}^\dagger$  ( $c_{i\sigma}$ ) is a creation (annihilation) operator of spin up/down ( $\sigma = \uparrow, \downarrow$ ) electrons on lattice site  $i$ ,  $n_{i\sigma} =$

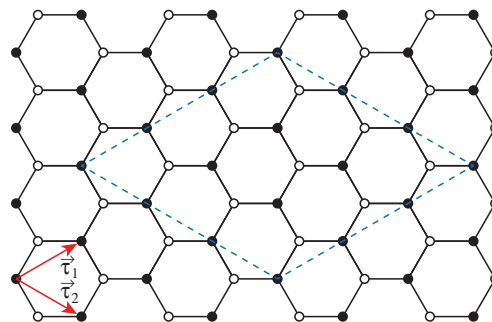


FIG. 1: **The honeycomb lattice.** Primitive lattice vectors  $\vec{\tau}_1$  and  $\vec{\tau}_2$  are denoted by red arrows. As an example, the honeycomb lattice with  $L = 3$  is indicated by dashed blue lines. Solid and open circles indicate sites on A and B sublattices, respectively.

$c_{i\sigma}^\dagger c_{i\sigma}$ , and  $t$  ( $U$ ) denotes the nearest-neighbor hopping (on-site repulsion). This is known to be a model Hamiltonian for graphene with  $U/t \approx 3$  [11]. More importantly, it is not geometrically frustrated, namely, as seen in Fig. 1, the neighboring sites of any site on A sublattice belong to B sublattice (and vice versa). Indeed, it is well known that the ground state becomes an antiferromagnetic insulator (AFMI), i.e., classically Néel ordered, from a semi-metal (SM) with increasing  $U/t$  [12].

Very recently, Meng *et al.* [2] has reexamined the ground state phase diagram of this model and found a possible spin liquid phase in the range  $3.4 \lesssim U/t \lesssim 4.3$  between SM and AFMI. Their finding is rather surprising because it is widely believed that a stable spin liquid occurs most likely in frustrated quantum systems where strong quantum fluctuations destroy the long-range magnetic order even at zero temperature [1]. Their study was particularly successful because, with the auxiliary field technique [13], there is no sign problem in the corresponding quantum Monte Carlo simulations, and an accurate

\*Electronic address: sorella@sissa.it

†Electronic address: otsukay@riken.jp

‡Electronic address: yunoki@riken.jp

finite size scaling was possible by using numerically exact results for clusters containing up to 648 sites. So far, their results represent the most important numerical evidence for a possible spin liquid ground state in a "realistic" electronic model in two dimensions (2D), because, to our knowledge, only a particularly simplified quantum dimer model on the triangular lattice [9] and the Kitaev model [10], built *ad hoc* to have an exact solution, allow a spin liquid ground state in 2D. Furthermore, their results were considered to be a clear violation of the "Murphy's Law": in a too simple model, not vexed by the "fermion sign problem", nothing interesting can occur [5].

Here, by performing simulations for much larger clusters containing up to 2592 sites, we show that antiferromagnetic order concomitantly occurs once the insulating behavior sets in, supporting the more conventional Hartree-Fock (HF) transition from SM to AFMI [12]. Although our results agree with the previous study for the same clusters up to 648 sites, we have reached a quite different conclusion, as the possible spin liquid region reduces substantially to a small interval  $3.8t \lesssim U/t \lesssim 3.9t$ , if it ever exists. This reminds us similar claims on spin liquid behaviors in different systems in 2D [14, 15], which have been corrected later on by much larger cluster simulations, showing instead antiferromagnetic long-range order [16, 17].

## Results

We use finite size clusters of  $N = 2L^2$  sites (thus containing  $L \times L$  unit cells) with periodic boundary conditions (see Fig. 1), which satisfy all symmetries of the infinite lattice [18] (also see Supplementary information). Here  $L$  is the linear dimension of the cluster and we take  $L$  up to 36. We use the well established auxiliary field Monte Carlo technique [13], which allows the statistical evaluation of the following quantity,

$$O(\tau) = \frac{\langle \psi_L | e^{-\frac{\tau}{2}\hat{H}} \hat{O} e^{-\frac{\tau}{2}\hat{H}} | \psi_R \rangle}{\langle \psi_L | e^{-\tau\hat{H}} | \psi_R \rangle}, \quad (2)$$

where  $\hat{O}$  is a physical operator,  $|\psi_R\rangle$  ( $|\psi_L\rangle$ ) is the right (left) trial wave function (not orthogonal to the exact ground state), and  $\tau$  is the projection time. The exact ground state expectation value  $\langle \hat{O} \rangle$  of the operator  $\hat{O}$  is then obtained by adopting the limit of  $\tau \rightarrow \infty$  and  $\Delta\tau \rightarrow 0$  for  $O(\tau)$ , where  $\Delta\tau$  is the short time discretization of  $\tau$ . This approximation – the so called Trotter approximation – is necessary to introduce the auxiliary fields [13] and implies a systematic error, negligible for small  $\Delta\tau$  (see Supplementary information).

First, we study both the spin structure factor  $S_{\text{AF}} = \frac{1}{N} \langle [\sum_{\mathbf{r}} (\mathbf{S}_{\mathbf{r},\text{A}} - \mathbf{S}_{\mathbf{r},\text{B}})]^2 \rangle$  and the spin-spin correlations  $C_s(\mathbf{R}) = \langle \mathbf{S}_{\mathbf{r},\text{A}} \cdot \mathbf{S}_{\mathbf{r}+\mathbf{R},\text{A}} \rangle$  at the maximum distance  $|\mathbf{R}| = L_{\text{max}}$  of each cluster for  $U/t = 4$ , where the strongest evidence of a spin liquid behavior was found in Ref. 2. Here  $\mathbf{S}_{\mathbf{r},\text{A}}$  ( $\mathbf{S}_{\mathbf{r},\text{B}}$ ) is the spin operator at unit cell

$\mathbf{r}$  on A (B) sublattice. As shown in Fig. 2b, our results show consistently a finite value of the antiferromagnetic order parameter  $m_s^2 = S_{\text{AF}}/N = C(L_{\text{max}})$  for  $L \rightarrow \infty$ , in sharp contrast to the existence of a spin liquid, i.e., spin disordered, ground state reported in Ref. 2.

By doing similar calculations for several  $U/t$  values (see Fig. 2 and Supplementary information), we find in Fig. 3 that  $m_s$  approximately scales linearly with respect to  $U/t$ , i.e.,  $m_s \propto |U - U_c|^\beta$ , with a critical exponent  $\beta \simeq 0.8$ , which is similar to the critical behavior ( $\beta = 1$ ) predicted by the HF theory [12]. Although corrections to this almost linear critical behavior are obviously expected, they do not change much the critical value  $U_c$  at which the antiferromagnetic order melts, as clearly shown in Fig. 3. Our best estimate of the critical value is  $U_c/t = 3.869 \pm 0.013$ , which is much smaller than the one ( $\approx 4.3$ ) reported in Ref. 2. Note, however, that the critical exponent  $\beta$  may be different from the present estimate if the critical region is very close to  $U_c$ . In such case the accurate determination of  $\beta$  obviously requires much larger clusters which are not feasible at present.

Let us now evaluate the spin gap  $\Delta_s$ . In order to avoid possible errors in extrapolating the imaginary time displaced spin-spin correlation functions, here we calculate directly the total energies in the singlet and the triplet sectors, with improved estimators, which dramatically reduce their statistical errors [20] (also see Supplementary information). We can see clearly in Fig. 4a that the extrapolated spin gaps for different  $U/t$  values are always zero within statistical errors (e.g., the statistical error as small as  $0.004t$  for  $U/t = 4$ ).

Next, we investigate whether the system is metallic or insulating, namely, whether there exists a zero or a finite charge gap. For this purpose, it is enough to simply study the long distance behavior of charge-charge correlations,  $\rho(\mathbf{R}) = \langle n_{\mathbf{r},\text{A}} n_{\mathbf{r}+\mathbf{R},\text{A}} \rangle - \langle n_{\mathbf{r},\text{A}} \rangle \langle n_{\mathbf{r}+\mathbf{R},\text{A}} \rangle$ . Here  $n_{\mathbf{r},\text{A}}$  is the density operator at unit cell  $\mathbf{r}$  on A sublattice (see Fig 1). They should change from power law to exponential behavior at a critical  $U$  where the charge gap opens up. This change of behavior is evident in Fig. 4b and appears consistently around the onset of the antiferromagnetic transition ( $U_c$ ), within a remarkably small uncertainty  $< 0.1t$  on the value of  $U$ . Our results therefore strongly support the more conventional scenario of a direct and continuous quantum phase transition between SM and AFMI [12].

## Discussion

Let us now discuss here why we have not found any evidence of a spin liquid phase. As shown in Ref. 21, by applying one of the theorems by Lieb [22], it is easily proved that the exact ground state of this model for  $U \neq 0$  satisfies the Marshall sign rule [23] in the sector of no doubly occupied sites, accounting for low energy spin excitations. Indeed, the phases coincide with those of the simple antiferromagnetic

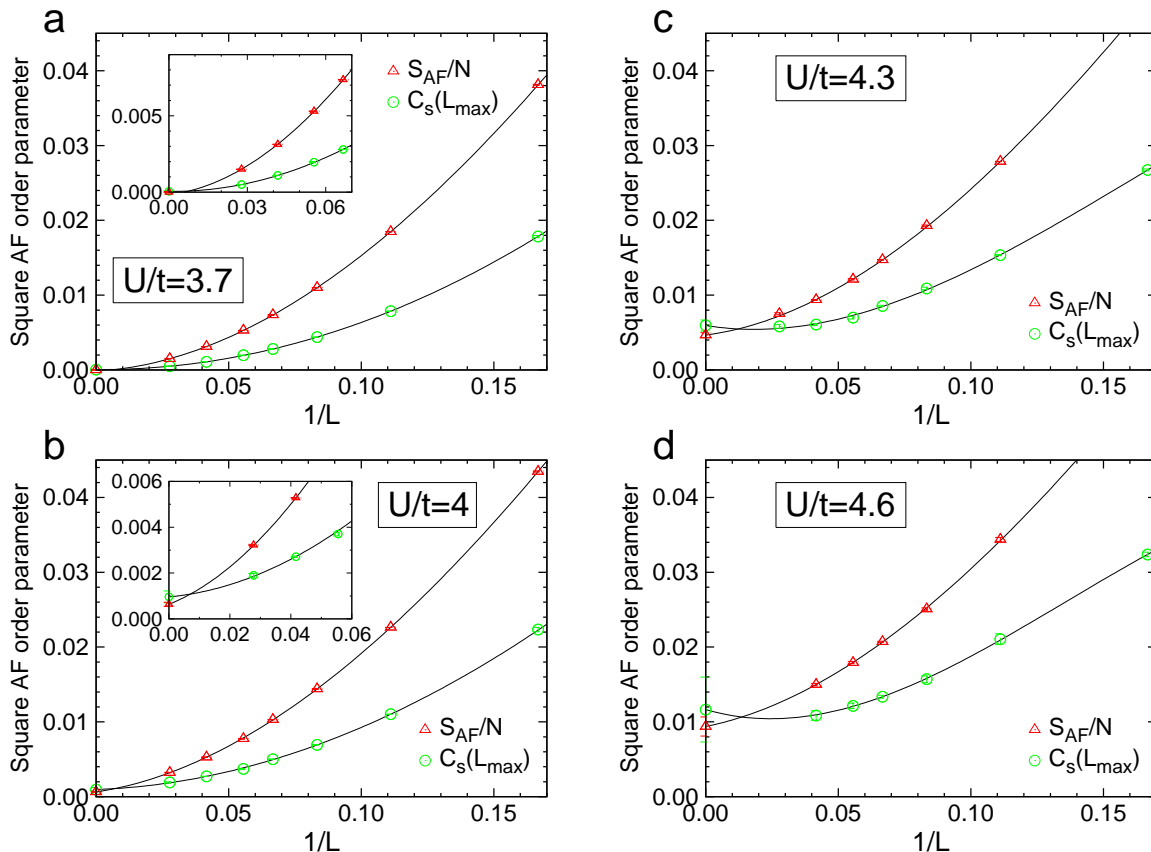


FIG. 2: **Finite size scaling of spin-spin correlation functions for the Hubbard model on the honeycomb lattice at half-filling.** Spin structure factor,  $S_{AF}$ , and spin-spin correlations at the maximum distance,  $C_s(L_{\max})$ , are denoted by triangles and circles, respectively. Here,  $L$  is the linear size of clusters containing  $N = 2L^2$  sites. Antiferromagnetic order parameter squared,  $m_s^2$ , is estimated by finite size extrapolating  $S_{AF}$  and  $C_s(L_{\max})$  to  $L \rightarrow \infty$ , namely,  $m_s^2 = \lim_{L \rightarrow \infty} S_{AF}/N = \lim_{L \rightarrow \infty} C_s(L_{\max})$ . Solid curves are fit of the data by cubic polynomials in  $1/L$ . It is clearly seen that a consistent extrapolated value  $m_s^2$  is obtained for both quantities  $S_{AF}$  and  $C_s(L_{\max})$ , indicated respectively by triangles and circles at  $1/L = 0$ . Error bars of the extrapolated values are computed with a resampling technique described in Methods. Insets show the expanded plots for large  $L$ . The fits are stable upon removal of the data for the largest (i.e.,  $L = 36$ ) or the smallest (i.e.,  $L = 6$ ) size, and the extrapolated value of  $C_s(L_{\max})$  is always consistent with  $S_{AF}/N$  within two standard deviations. Including the largest size calculations in the fits increases the extrapolated values slightly and at the same time gives more consistent values of  $C_s(L_{\max})$  and  $S_{AF}/N$  in  $L \rightarrow \infty$ , thus clearly indicating that our present estimate provides an accurate lower bound for the AF order parameter  $m_s$ . All data presented in this figure refers to  $\Delta\tau t = 0.1$ , because the Trotter  $\Delta\tau$  error is essentially negligible (see Fig. 3). More details are found in Supplementary information.

Néel state ordered along the  $x$ -spin quantization axis,  $\prod_{\mathbf{R} \in A} (|\uparrow\rangle_{\mathbf{R}} - |\downarrow\rangle_{\mathbf{R}}) \prod_{\mathbf{R} \in B} (|\uparrow\rangle_{\mathbf{R}} + |\downarrow\rangle_{\mathbf{R}})$ , where  $|\uparrow\rangle_{\mathbf{R}}$  and  $|\downarrow\rangle_{\mathbf{R}}$  are spin configurations (along the  $z$ -spin quantization axis) at site  $\mathbf{R}$ . The expansion of this state in terms of  $|\uparrow\rangle_{\mathbf{R}}$  and  $|\downarrow\rangle_{\mathbf{R}}$  yields the simple Marshall sign, namely, it is negative if the number of spin down in the A sublattice is odd. Thus, the phases of the ground state are trivial in the bosonic spin 1/2 sector. Therefore, Bose-Einstein condensation can hardly be avoided and a magnetic long-range order occurs once the charge gap becomes finite.

At this point, one could be tempted to assume the general validity of the above observation for generic S=1/2 model Hamiltonians with SU(2) invariance and use this

criteria based on the phases of the ground state wave function as a powerful guideline in the search of spin liquids for model systems as well as for real materials. Indeed, in all unfrustrated spin-1/2 Heisenberg and Hubbard models in the sector of no doubly occupied sites, the phases of the ground state wave function are not at all entangled in real space as they factorize into independent contributions relative to each site. Instead, the phases of the ground state wave functions are highly non trivial in well established spin liquid models such as, for instance, the Kitaev's model [10], and the celebrated quantum dimer model on the triangular lattice [9], because they are described by paired wave functions, which couple in a non trivial way the phases of nearest neighbor spins [24].

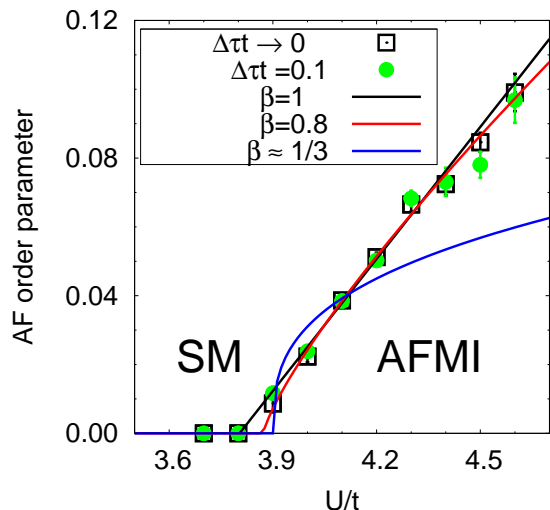


FIG. 3: **The ground state phase diagram for the half-filled Hubbard model on the honeycomb lattice.** Antiferromagnetic order parameter  $m_s$  (open squares) as a function of  $U/t$ . The error, due to the finite  $\Delta\tau$  in the evaluation of  $S_{AF}$ , is removed by quadratic extrapolations for  $\Delta\tau t = 0.1$ ,  $\Delta\tau t = 0.2$ , and  $\Delta\tau t = 0.4$  (see Supplementary information for details). The antiferromagnetic order parameter  $m_s$  is obtained by finite-size extrapolating the square root of  $S_{AF}/N$ ,  $m_s = \lim_{L \rightarrow \infty} \sqrt{S_{AF}/N}$ , as shown in Fig. 2. For comparison,  $m_s$  estimated by finite-size extrapolating  $S_{AF}$  for  $\Delta\tau t = 0.1$  without the  $\Delta\tau$  correction is also plotted (solid circles). SM and AFMI stand for semi-metal and antiferromagnetic insulator, respectively. Solid lines are fit of  $m_s$  with the critical behavior  $m_s = (U_c - U)^\beta$ , for selected critical exponents  $\beta$ .  $\beta = 1$  for the HF theory [12],  $\beta = 0.3362$  for the classical critical theory of quantum magnets [19], and  $\beta = 0.80 \pm 0.04$  is the best fit of our data. In any case, the critical  $U_c$  ranges from  $U_c/t = 3.8$  ( $\beta = 1$ ) to  $U_c/t = 3.9$  ( $\beta = 0.3362$ ). Our best estimate is  $U_c/t = 3.869 \pm 0.013$ .

Therefore, we conclude that in a true spin liquid in 2D, the phases of the ground state wave function should be highly non trivial and entangled, otherwise any seed of spin liquid behavior would be most likely destabilized. To our best knowledge, the above observation is valid so far for all spin-1/2 models with  $SU(2)$  invariance. Notice that the restriction to  $SU(2)$  invariant models appears to be important because the spin-1/2 easy-axis Heisenberg model on the Kagome lattice most likely display spin liquid behavior [25–27]. Here, however, the calculations have not been confirmed on fairly low temperatures yet. Therefore, further numerical study is required for understanding what are the key ingredients that stabilize a spin liquid phase in "realistic" electronic models.

## Methods

Here we employ the standard auxiliary field Monte Carlo algorithm [13] with a more efficient implementation [20] by using different left and right trial functions  $|\psi_L\rangle$  and  $|\psi_R\rangle$  in equation (16). We include also in the trial wave function a Gutzwiller type projection,  $\exp(-g \sum_i n_{i\uparrow} n_{i\downarrow})$ , where  $g$  is the Gutzwiller variational parameter, to optimize the efficiency. As reported in Ref. 20, the statistical error in evaluating the energy  $E(S)$  for a given spin  $S$  is dramatically reduced for appropriate values of  $g$ . Thus we can evaluate the spin gap  $\Delta_S = E(S=1) - E(S=0)$  with high accuracy, without facing the negative sign problem, by directly simulating the singlet  $S=0$  and the triplet  $S=1$  sectors separately (see Supplementary information).

In order to accelerate the convergence to the ground state, we use for  $|\psi_R\rangle$  a Slater determinant with a definite spin  $S$ , by breaking only spatial symmetries to remove the degeneracy at momenta  $K$  and  $K'$  for the clusters chosen (a similar strategy was adopted in Ref. 2). Conversely, we use for  $|\psi_L\rangle$  a rotational and translationally invariant Slater determinant obtained by diagonalizing a mean field Hamiltonian, containing an explicit antiferromagnetic order parameter directed along the  $x$ -spin quantization axis. In this way, the left and the right trial wave functions break different symmetries (spin and spatial ones, respectively), and for any symmetric operator  $\hat{O}$  the convergence to the ground state is expected to be much faster because it is dominated by the singlet gap in the symmetric sector  $\Delta_{\text{gap}}$ , that is clearly much larger than, e.g., the lowest triplet excitation in the magnetic phase. Since  $\Delta_{\text{gap}}$  is expected to scale to zero (if indeed zero) at most as  $\simeq 1/L$ , we use a projection time  $\tau = (L+4)/t$ , which we have tested carefully to be large enough for well converged results (see Supplementary information). We have also checked that the systematic error due to discretizing  $\tau$  is basically negligible with  $\Delta\tau t = 0.14$  for the spin gap calculations and with  $\Delta\tau t = 0.1$  for the correlation functions (see Fig. 3 and Supplementary information).

In order to evaluate the statistical errors of the finite size extrapolations, we use a straightforward resampling technique. This resampling technique is used, for example, when values of  $S_{AF}$  calculated for finite sizes are extrapolated to  $L \rightarrow \infty$  to estimate  $m_s$  in Fig. 3. Let us denote in general the calculated Monte Carlo data  $f(L)$  and the corresponding statistical error  $\delta f(L)$  obtained for a cluster of size  $L$ . The main goal of this resampling technique is to estimate the finite-size extrapolated value  $c_0$  and its statistical error  $\delta c_0$  when the Monte Carlo data are fitted by, e.g., cubic polynomials,

$$f(L) = \sum_{n=0}^3 \frac{c_n}{L^n}. \quad (3)$$

In this resampling technique, we first generate for each  $L$  a "fictitious sample" which is normally distributed

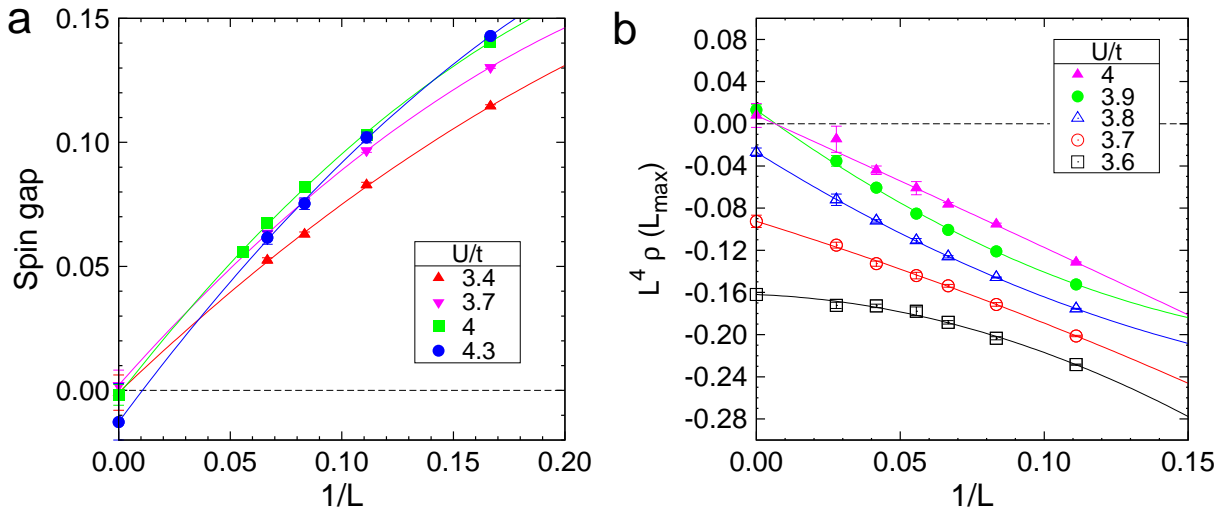


FIG. 4: **Finite size scaling of spin gap and charge-charge correlation functions for the Hubbard model on the honeycomb lattice at half-filling.** **a**, Spin gap  $\Delta_s = E(S = 1) - E(S = 0)$  for various  $U/t$ , where  $E(S)$  is the lowest energy for a given spin  $S$ . Solid curves are fits of data by quadratic polynomials in  $1/L$ . The extrapolated values are also indicated at  $1/L = 0$ . Error bars of the extrapolated values are computed with the resampling technique. In the semi-metallic region, the spin gap scales to zero with increasing the resolution in momentum space, namely as  $1/L$ . In the antiferromagnetic region, the spin gap should instead vanish as  $1/L^2$ . This explains why for  $U/t = 4.3$  the gap extrapolates to negative values, as we are well inside the antiferromagnetic phase (see Fig. 3). In any case, a sizable spin gap is not found for any value of  $U/t$ . **b**, Charge-charge correlation function  $\rho(\mathbf{R}) = \langle n_{r,A} n_{r+\mathbf{R},A} \rangle - \langle n_{r,A} \rangle \langle n_{r+\mathbf{R},A} \rangle$  at the maximum distance  $|\mathbf{R}| = L_{\max}$  for several values of  $U/t$ . In the semi-metallic phase,  $\rho(\mathbf{R}) \sim 1/R^4$  and  $L^4 \rho(L_{\max})$  should converge to a finite value for  $L \rightarrow \infty$ . Instead, when a charge gap opens, the charge-charge correlations should decay exponentially and  $L^4 \rho(L_{\max})$  converges to zero in this limit. Indeed, a quadratic extrapolation to  $L \rightarrow \infty$  of this quantity, which is clearly appropriate in the semi-metallic phase, appears to vanish in the interval between  $U/t = 3.8$  and  $U/t = 3.9$ , in remarkable agreement with the critical value  $U_c = 3.869 \pm 0.013$  estimated for the antiferromagnetic transition (see Fig. 3). Obviously, a polynomial fit is not consistent in the insulating region and this explains why the extrapolated value to  $1/L = 0$  seems slightly positive in this case. For the spin gap and the charge-charge correlation functions, the Trotter  $\Delta\tau$  error is negligible, and all data shown here refers to  $\Delta\tau t = 0.14$  and  $0.1$ , respectively.

around  $f(L)$  with its standard deviation  $\delta f(L)$ , which is also an output of the quantum Monte Carlo simulation. Then, we fit these "fictitious" data to equation (3), by using the weighted (with  $1/(\delta f(L))^2$ ) least square fit, and estimate  $c_0$ . We repeat this  $M_{rs}$  times so that we have now  $M_{rs}$  numbers of samples for  $c_0$ , i.e.,  $\{c_0^{(1)}, c_0^{(2)}, \dots, c_0^{(M_{rs})}\}$  distributed according to a probability distribution consistent with the Monte Carlo simulations. Finally, we simply average  $\{c_0^{(i)}\}$  ( $i = 1, 2, \dots, M_{rs}$ ) for  $\langle c_0 \rangle = \lim_{L \rightarrow \infty} f(L)$ , and the standard deviation of  $\{c_0^{(i)}\}$  gives an estimate of the statistical error  $\delta c_0$  of the extrapolated value  $\langle c_0 \rangle$ . We take  $M_{rs} = 200$ . We have checked that the resultant  $\langle c_0 \rangle$  and  $\delta c_0$  are not dependent on  $M_{rs}$  as long as  $M_{rs}$  is large enough.

#### Acknowledgments

We acknowledge E. Tosatti, F. Becca, and T. Li for useful discussions. We are also grateful to A. Muramatsu

and F. F. Assaad for valuable comments and providing us some of their numerical data reported in Ref. 2. This work is supported by a PRACE grant 2010PA0447 and by MIUR-COFIN2012. Part of the results is obtained by the K computer at RIKEN Advanced Institute for Computational Science.

#### Additional information

The authors declare no competing financial interests. Supplementary information accompanies this paper on [www.nature.com/naturephysics](http://www.nature.com/naturephysics). Reprints and permissions information is available online at [www.nature.com/scientificreports](http://www.nature.com/scientificreports). Correspondence and requests for materials should be addressed to S.S or S.Y.

- 
- [1] Balents, L. Spin liquids in frustrated magnets. *Nature* **464**, 199–208 (2010).
- [2] Meng, Z. Y., Lang, T. C., Wessel, S., Assaad, F. F. & Muramatsu, A. quantum spin liquid emerging in two-dimensional correlated Dirac fermions. *Nature* **464**, 847–851 (2010).
- [3] Yan, S., Huse, D. A. & White, S. R. Spin-liquid ground state of the  $S = 1/2$  Kagome Heisenberg antiferromagnet. *Science* **332**, 1173–1176 (2011).
- [4] Jiang, H.-C., Yao, H. & Balents, L. Spin liquid ground state of the spin-1/2 square  $J_1$ - $J_2$  Heisenberg model. *Phys. Rev. B* **86**, 024424 (2012).
- [5] Kivelson S. A. Spin liquid ground states? <http://www.condmatjournalclub.org/?p=1251> (2011).
- [6] Shimizu, Y., Miyagawa, K., Kanoda, K., Maesato, M., Saito, G. Spin liquid state in an organic Mott insulator with a triangular lattice. *Phys. Rev. Lett.* **91**, 107001 (2003).
- [7] Kurosaki, Y., Shimizu, Y., Miyagawa, K., Kanoda, K., & Saito, G. Mott transition from s spin liquid to a Fermi liquid in the spin-frustrated organic conductor  $\kappa$ -(ET)<sub>2</sub>Cu<sub>2</sub>(CN)<sub>3</sub>. *Phys. Rev. Lett.* **95**, 177001 (2005).
- [8] Itou, T., Oyamada, A., Maegawa, S., Tamura, M., & Kato, R. Quantum spin liquid in the spin-1/2 triangular antiferromagnet EtMe<sub>3</sub>Sb[Pd(dmit)<sub>2</sub>]<sub>2</sub>. *Phys. Rev. B* **77**, 104413 (2008).
- [9] Fendley, P., Moessner, R., & Sondhi, S. L. Classical dimers on the triangular lattice. *Phys. Rev. B* **66**, 214513 (2002).
- [10] Kitaev, A. Anyons in an exactly solved model and beyond, *Annals of Physics* **321**, 2–111 (2006).
- [11] Castro Neto, A. H., Guinea, F., Peres, N. M. R., Novoselov, K. S. & Geim, A. K. The electronic properties of graphene, *Rev. Mod. Phys.* **81**, 109–162 (2009).
- [12] Sorella, S. & Tosatti, E. Semimetal-insulator transition of the Hubbard model in the honeycomb lattice. *Europhys. Lett.* **19**, 699–704 (1992).
- [13] Hirsch, J. E. Two dimensional Hubbard model: numerical simulation study. *Phys. Rev. B* **31**, 4403–4419 (1985).
- [14] Santoro, G., Sorella, S., Guidoni, L., Parola, A. & Tosatti, E. Spin-liquid ground state in a two-dimensional nonfrustrated spin model. *Phys. Rev. Lett.* **83**, 3065–3068 (1999).
- [15] Parola, A. , Sorella, S., & Zhong, Q. F. Realization of a spin liquid in a two dimensional quantum antiferromagnet, *Phys. Rev. Lett.* **71**, 4393–4396 (1993).
- [16] Harada, K., Kawashima, N. & Troyer, M. Néel and spin-Peierls ground states of two-dimensional  $SU(N)$  quantum antiferromagnets. *Phys. Rev. Lett.* **90** 117203 (2003).
- [17] Sandvik, A. W. Multichain mean-field theory of quasi-one-dimensional quantum spin systems, *Phys. Rev. Lett.* **83**, 3069–3072 (1999).
- [18] Bernu, B., Lecheminant, P., Lhuillier, C. & Pierre, L. Exact spectra, spin susceptibilities, and order parameter of the quantum Heisenberg antiferromagnet on the triangular lattice. *Phys. Rev. B* **50**, 10048–10062 (1994).
- [19] Guida, R. & Zinn-Justin, J. Critical exponents of the N-vector model. *J. Phys. A* **31**, 8103–8121 (1998).
- [20] Hlubina, R., Sorella, S. & Guinea, F. Ferromagnetism in the two dimensional t-t Hubbard model at the Van Hove density. *Phys. Rev. Lett.* **78**, 1343–1346 (1997).
- [21] Li, T. Absence of topological degeneracy in the Hubbard model on honeycomb lattice. *Europhys. Lett.* **93**, 37007 (2011).
- [22] Lieb, E. H. Two theorems on the Hubbard model. *Phys. Rev. Lett.* **62**, 1201–1204 (1989).
- [23] Marshall, W. Antiferromagnetism. *Proc. R. Soc. London Ser. A* **232**, 48–68 (1955).
- [24] Yunoki, S. & Sorella, S. Two spin liquid phases in the spatially anisotropic triangular Heisenberg model, *Phys. Rev. B* **74**, 014408 (2006).
- [25] Balents, L., Fisher, M. P. A. & Girvin, S. M. Fractionalization in an easy-axis Kagome antiferromagnet, *Phys. Rev. B* **65**, 224412 (2002).
- [26] Isakov, S. V., Hastings, M. B. & Melko, R. G. Topological entanglement entropy of a Bose-Hubbard spin liquid, *Nature Physics*, **7**, 772–775 (2011).
- [27] Isakov, S. V., Melko, R. G. & Hastings, M. B. Universal signatures of fractionalized quantum critical points, *Science*, **13**, 193–195 (2012).

## Supplementary information

In this Supplementary information, we explain details of the trial wave functions used and provide numerical data for correlation functions and spin gap of the half-filled Hubbard model on the honeycomb lattice. The Hubbard model is described by the following Hamiltonian:

$$\hat{H} = -t \sum_{\langle \mathbf{R}, \mathbf{R}' \rangle, \sigma} \left( c_{\mathbf{R}, \sigma}^\dagger c_{\mathbf{R}', \sigma} + \text{h.c.} \right) + U \sum_{\mathbf{R}} n_{\mathbf{R}, \uparrow} n_{\mathbf{R}, \downarrow}, \quad (4)$$

where  $c_{\mathbf{R}, \sigma}^\dagger$  is an electron creation operator at site  $\mathbf{R}$  with spin  $\sigma = (\uparrow, \downarrow)$ ,  $n_{\mathbf{R}, \sigma} = c_{\mathbf{R}, \sigma}^\dagger c_{\mathbf{R}, \sigma}$ , and  $\langle \mathbf{R}, \mathbf{R}' \rangle$  runs over all nearest neighbor sites  $\mathbf{R}$  and  $\mathbf{R}'$ . Here the electron hopping is described by the first term ( $\hat{H}_0$ ) and the on-site Coulomb interaction is represented by the second term ( $\hat{H}_1$ ).

### I. HONEYCOMB LATTICE

As shown in Fig. 5a, the honeycomb lattice is formed by the primitive lattice vectors (with lattice constant  $a = 1$ ):

$$\vec{\tau}_1 = (3/2, \sqrt{3}/2) \quad (5)$$

$$\vec{\tau}_2 = (3/2, -\sqrt{3}/2). \quad (6)$$

Each unit cell contains two sites, belonging to different sublattices (A and B sublattices), and using  $\vec{\tau}_1$  and  $\vec{\tau}_2$  these sites are defined by

$$\mathbf{R}_A = n\vec{\tau}_1 + m\vec{\tau}_2 \quad (7)$$

$$\mathbf{R}_B = (n - 1/3)\vec{\tau}_1 + (m - 1/3)\vec{\tau}_2, \quad (8)$$

$$(9)$$

where  $n$  and  $m$  are integers. Periodic boundary conditions are obtained simply by requiring equivalence of lattice points when they differ by the lattice vectors  $\mathbf{T}_1$  and  $\mathbf{T}_2$  which define the lattice:

$$\mathbf{T}_1 = L\vec{\tau}_1 \quad (10)$$

$$\mathbf{T}_2 = L\vec{\tau}_2. \quad (11)$$

The lattice thus contains  $N = 2L^2$  independent sites, and satisfies all point group symmetries of the infinite lattice [1]. We have chosen  $L$  to be a multiple of 3. For this reason, two sites at the maximum distance  $L_{\max} = L$  in a given finite lattice are in the same sublattice, and are separated by a lattice vector

$$\vec{\tau}_{\max} = \frac{L}{3}(\vec{\tau}_1 + \vec{\tau}_2). \quad (12)$$

This maximum distance vector differs slightly from the one defined in Ref. 2 because here we consider also the rotation symmetry of 120 degrees around each site. This

symmetry is important in order to define properly the maximum distance possible in a given finite lattice among all equivalent ones.

The reciprocal lattice vectors in momentum space are given by

$$\vec{g}_1 = 2\pi(1/3, 1/\sqrt{3}) \quad (13)$$

$$\vec{g}_2 = 2\pi(1/3, -1/\sqrt{3}), \quad (14)$$

and using these vectors a momentum  $\vec{k}$  in a given finite lattice of  $N = 2L^2$  is described by

$$\vec{k} = \frac{k_1}{L}\vec{g}_1 + \frac{k_2}{L}\vec{g}_2, \quad (15)$$

where  $k_1, k_2 = 0, 1, \dots, L - 1$ . Thus, only when  $L$  is a multiple of 3, the high symmetric momenta K:  $2\pi(1/3, 1/3\sqrt{3})$  and K':  $2\pi(1/3, -1/3\sqrt{3})$  are allowed (see in Fig. 5b). These are the momenta where Dirac points appear and in our study we choose  $L$  to be a multiple of 3 for the systematic finite-size scaling analysis.

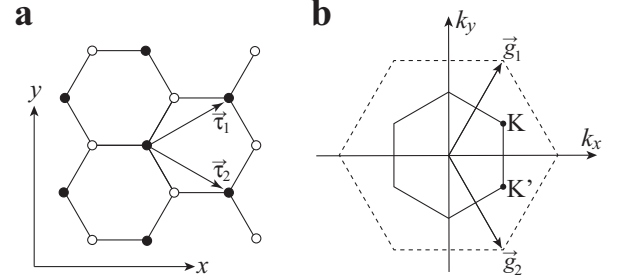


FIG. 5: (a) The honeycomb lattice with the primitive lattice vectors  $\vec{\tau}_1 = (3/2, \sqrt{3}/2)$  and  $\vec{\tau}_2 = (3/2, -\sqrt{3}/2)$ . Each unit cell contains two sites (indicated by open and solid circles) belonging to A and B sublattices. (b) The first Brillouin zone (denoted by solid lines forming hexagon) in the momentum space with the reciprocal lattice vectors  $\vec{g}_1 = 2\pi(1/3, 1/\sqrt{3})$  and  $\vec{g}_2 = 2\pi(1/3, -1/\sqrt{3})$ . Two high symmetric and independent momenta are indicated by K:  $2\pi(1/3, 1/3\sqrt{3})$  and K':  $2\pi(1/3, -1/3\sqrt{3})$ . K and K' are allowed only when  $L$  is a multiple of 3 for a finite lattice of  $N = 2L^2$  with periodic boundary conditions.

### II. TRIAL WAVE FUNCTIONS

We use the auxiliary field quantum Monte Carlo technique [3] to statistically evaluate

$$O(\tau) = \frac{\langle \psi_L | e^{-\frac{\tau}{2}\hat{H}} \hat{O} e^{-\frac{\tau}{2}\hat{H}} | \psi_R \rangle}{\langle \psi_L | e^{-\tau\hat{H}} | \psi_R \rangle}, \quad (16)$$

where  $\hat{O}$  is a physical operator and  $\tau$  is the projection time.  $|\psi_R\rangle$  and  $|\psi_L\rangle$  are respectively the right and the left trial wave functions, which are not orthogonal to the exact ground state wave function. The exact ground state expectation value  $\langle \hat{O} \rangle$  of the operator  $\hat{O}$  is then obtained

by adopting the limit of  $\tau \rightarrow \infty$  and  $\Delta\tau \rightarrow 0$  for  $O(\tau)$ , where  $\Delta\tau$  is the short time discretization of  $\tau$  introduced in the Suzuki-Torotter decomposition [4]

$$e^{-\tau\hat{H}} = \left[ e^{-\frac{1}{2}\Delta\tau\hat{H}_0} e^{-\Delta\tau\hat{H}_1} e^{-\frac{1}{2}\Delta\tau\hat{H}_0} + \mathcal{O}\left((\Delta\tau)^3\right) \right]^{N_\tau} \quad (17)$$

with  $\tau = N_\tau\Delta\tau$ . As shown in Fig. 6, the systematic error introduced in this decomposition is negligible for small  $\Delta\tau$ . Notice also that the decomposition adopted here is symmetric, thus allowing an  $O(\Delta\tau^3)$  error in the short time propagation (the non-symmetric form,  $e^{-\Delta\tau\hat{H}} \approx e^{-\Delta\tau\hat{H}_0} e^{-\Delta\tau\hat{H}_1}$ , has a much larger error  $O(\Delta\tau^2)$ ). Therefore, we can use larger  $\Delta\tau$  with excellent accuracy. Indeed, we find that  $\Delta\tau t = 0.14$  (0.1) is small enough to ignore the systematic errors for the spin gap (spin and charge correlation) calculations.

In our calculations, the left trial function  $|\psi_L\rangle$  is given by

$$|\psi_L\rangle = \hat{P}_G |\Phi_{\text{MF}}\rangle, \quad (18)$$

where  $\hat{P}_G$  is the Gutzwiller projection

$$\hat{P}_G = \prod_{\mathbf{R}} \exp(-g n_{\mathbf{R},\uparrow} n_{\mathbf{R},\downarrow}), \quad (19)$$

and  $|\Phi_{\text{MF}}\rangle$  is the  $N$ -electron ground state of the following mean field Hamiltonian:

$$\begin{aligned} \hat{H}_{\text{MF}} = & - \sum_{\langle \mathbf{R}, \mathbf{R}' \rangle} \sum_{\sigma} \left( c_{\mathbf{R},\sigma}^\dagger c_{\mathbf{R}',\sigma} + \text{h.c.} \right) \\ & + \Delta \sum_{\mathbf{R}} (-1)^{s(\mathbf{R})} \left( c_{\mathbf{R},\uparrow}^\dagger c_{\mathbf{R},\downarrow} + c_{\mathbf{R},\downarrow}^\dagger c_{\mathbf{R},\uparrow} \right), \quad (20) \end{aligned}$$

with  $\Delta$  being the antiferromagnetic order parameter, and  $s(\mathbf{R}) = 0$  (1) if site  $\mathbf{R}$  belongs to the A (B) sublattice. Obviously,  $|\psi_L\rangle$  breaks the  $SU(2)$  spin rotational symmetry, but conserves the spatial rotational symmetry. In order to obtain a rapid convergence with respect to  $\tau$  in Eq. (16), we use optimized values of  $g$  and  $\Delta$  which maximize  $\langle \psi_L | e^{-\tau\hat{H}} | \psi_L \rangle / \langle \psi_L | \psi_L \rangle$ .

For the right trial wave function  $|\psi_R\rangle$ , we simply use a Slater determinant constructed by the single-particle states of the non-interacting  $\hat{H}_0$  (with eigenstates  $\varepsilon_{\mathbf{k}}$ ), occupied from the lowest energy states by  $N_\uparrow$  number of up electrons and  $N_\downarrow$  number of down electrons with  $N_\uparrow = N_\downarrow = N/2$  for the spin singlet ( $S = 0$ ) and  $N_\uparrow - 1 = N_\downarrow + 1 = N/2$  for the spin triplet ( $S = 1$ ). In order to remove the open shell condition in the single-particle energy level  $\varepsilon_{\mathbf{k}}$  at the Fermi level and thus to avoid the negative sign problem, we add to  $\hat{H}_0$  an appropriate small perturbative term. For example, to remove the degeneracy at momenta  $K$  and  $K'$ , a tiny perturbation term  $\delta t \sum_{\mathbf{R},\sigma} \left( c_{\mathbf{R},\sigma}^\dagger c_{\mathbf{R},\sigma} c_{\mathbf{R}-\vec{\tau}_{AB},\sigma} + \text{h.c.} \right)$  with  $\vec{\tau}_{AB} = \frac{1}{3}(\vec{\tau}_1 + \vec{\tau}_2)$  is added to  $\hat{H}_0$ . This term certainly breaks the spatial rotational symmetry, but preserve exactly the spin rotational symmetry.

The left and the right trial wave functions therefore break different symmetries (spin and spatial rotations, respectively). An advantage of using these trial wave functions is that for any symmetric operator  $\hat{O}$  the convergence to the ground state is expected to be much faster in  $\tau$  because it is dominated by the singlet gap in the symmetric sector  $\Delta_{\text{gap}}$ , that is clearly much larger than, e.g., the lowest triplet excitation in the magnetic phase. Since  $\Delta_{\text{gap}}$  is expected to scale to zero (if indeed zero) at most as  $\simeq 1/L$ , we take a projection time  $\tau = (L + 4)/t$ , which, as shown below, is large enough for well converged results.

It should be emphasized that with these trial wave functions we are able to perform the quantum Monte Carlo simulations for the spin singlet and the spin triplet sectors independently with no negative sign problem. This is one of the crucial technical points in our simulations since we can estimate the spin gap directly and accurately. This should be contrasted to Ref. 2 where the estimation of the spin gap relies on the asymptotic behavior of the imaginary time displaced spin-spin correlation functions, which is sometime very difficult to extract accurately.

In addition, we use a "mixed average" for the energy calculations, i.e.,

$$\langle \hat{H} \rangle = \lim_{\tau \rightarrow \infty} \frac{\langle \psi_L | \hat{H} e^{-\tau\hat{H}} | \psi_R \rangle}{\langle \psi_L | e^{-\tau\hat{H}} | \psi_R \rangle}. \quad (21)$$

With this mixed average, we can significantly reduce the statistical error as compared to the one obtained with Eq. (16). The reduction of the statistical error is simply because this mixed average satisfies the zero variance principle, namely that the statistical error is zero if  $|\psi_L\rangle$  is exact.

### III. CORRELATION FUNCTIONS AND SPIN GAP

The spin-spin correlation functions at the maximum distance  $C_s(L_{\text{max}})$  is defined by

$$C_s(L_{\text{max}}) = \frac{1}{NN_{\vec{\tau}_{\text{max}}}} \sum_{\mathbf{R}, \vec{\tau}_{\text{max}}} \langle \mathbf{S}_{\mathbf{R}} \cdot \mathbf{S}_{\mathbf{R}+\vec{\tau}_{\text{max}}} \rangle, \quad (22)$$

where  $\mathbf{S}_{\mathbf{R}}$  is the spin operator at site  $\mathbf{R}$ ,  $\vec{\tau}_{\text{max}}$  runs over all symmetrically equivalent maximum distance vectors,  $N_{\vec{\tau}_{\text{max}}}$  is the number of these vectors, and  $L_{\text{max}} = |\vec{\tau}_{\text{max}}|$  [5]. As mentioned above, spins at site  $\mathbf{R}$  and site  $\mathbf{R} + \vec{\tau}_{\text{max}}$  are in the same sublattice. We also study the spin structure factor, which is defined by

$$S_{\text{AF}} = \frac{1}{N} \left\langle \left[ \sum_{\mathbf{r}} (\mathbf{S}_{\mathbf{r},A} - \mathbf{S}_{\mathbf{r},B}) \right]^2 \right\rangle, \quad (23)$$

where  $\mathbf{S}_{\mathbf{r},A}$  and  $\mathbf{S}_{\mathbf{r},B}$  are the spin operators at unit cell  $\mathbf{r}$  on A and B sublattices, respectively [5].



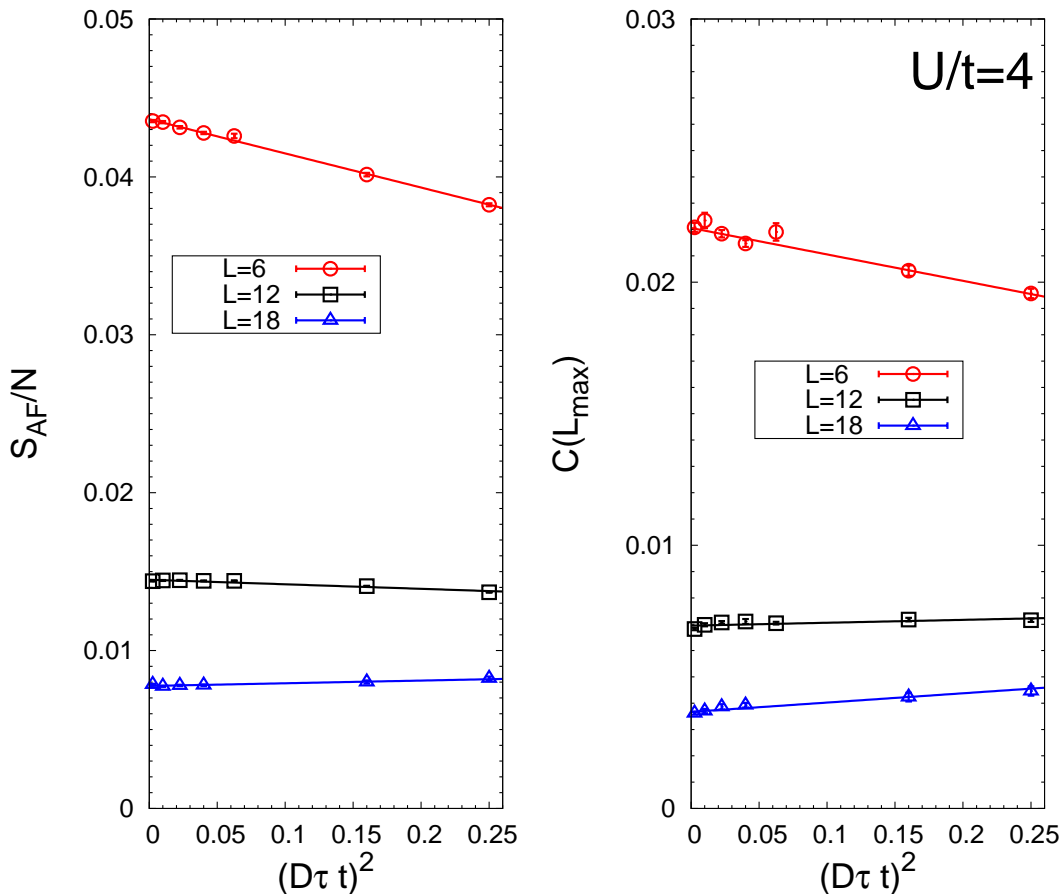


FIG. 6: Spin structure factor,  $S_{\text{AF}}$ , and spin-spin correlation functions at the maximum distance,  $C(L_{\text{max}})$ , as a function of the time discretization  $\Delta\tau$  used in the Trotter decomposition in Eq. (17) for  $U/t = 4$ . The system size  $L$  is indicated in the figures. The lines are linear fits of data in  $(\Delta\tau t)^2$ .

We first show in Fig. 7 the projection time  $\tau$  dependence of  $C_s(L_{\text{max}})$  and  $S_{\text{AF}}$  for  $L = 6$  and  $18$  with  $U/t = 4$ , and for  $L = 36$  with  $U/t = 3.9$ , which is very close to  $U_c/t \sim 3.87$ . Here, two different values of the antiferromagnetic order parameter  $\Delta$  in  $\hat{H}_{\text{MF}}$  [Eq. (20)] are chosen for the left trial function  $|\psi_L\rangle$  described by Eq. (18). We can clearly see in Fig. 7 that (i) both  $C_s(L_{\text{max}})$  and  $S_{\text{AF}}$  are well converged at  $\tau t = L + 4$  regardless of  $\Delta$  values and (ii) for the chosen  $\Delta$ 's the convergence of both quantities is always monotonically increasing within statistical errors, clearly showing that a finite projection time  $\tau$  can at most underestimate the magnetic order parameter.

TABLES I–IV (V–VIII) summarize  $C_s(L_{\text{max}})$  ( $S_{\text{AF}}/N$ ) calculated for different system sizes for several values of  $U/t$ . The thermodynamically extrapolated values for  $L \rightarrow \infty$  are also shown in these tables. The extrapolation is performed by fitting the calculated data with cubic polynomials in  $1/L$ , and the simple resampling method, explained in the Methods of the main text, is employed to estimate the statistical error of the extrapolated value. To check the stability of this

finite size extrapolation, we carry out three different cubic polynomial fitting, whenever possible, namely, by using (i) all data for  $L = 6, 12, 18, 24,$  and  $36$ , (ii) all data but without the largest size data ( $L = 36$ ), and (iii) all data but without the smallest size data ( $L = 6$ ). The results are shown in the last three rows of TABLES I–VIII. We can see in these table that these three different fits give quantitatively the same extrapolated results within the statistical error, strongly indicating that our fitting is indeed stable.

The antiferromagnetic order parameter  $m_s$  is obtained by  $m_s = \sqrt{S_{\text{AF}}/N} = \sqrt{C(L_{\text{max}})}$  for  $L \rightarrow \infty$ . Although  $C_s(L_{\text{max}})$  and  $S_{\text{AF}}$  are certainly different for a given finite  $L$ , the thermodynamically extrapolated values, namely  $m_s^2$ , are statistically consistent, as clearly seen in TABLES I–VIII. We also find that the general trend of the extrapolation in the thermodynamic limit  $L \rightarrow \infty$  is that the order parameter  $m_s$  estimated slightly increases if we remove the smallest sizes in the fit. This trend is also particularly evident even when quadratic polynomial is used for fitting data (not reported). This suggests that our estimated values  $m_s$  plotted in Fig. 3 of the main text and

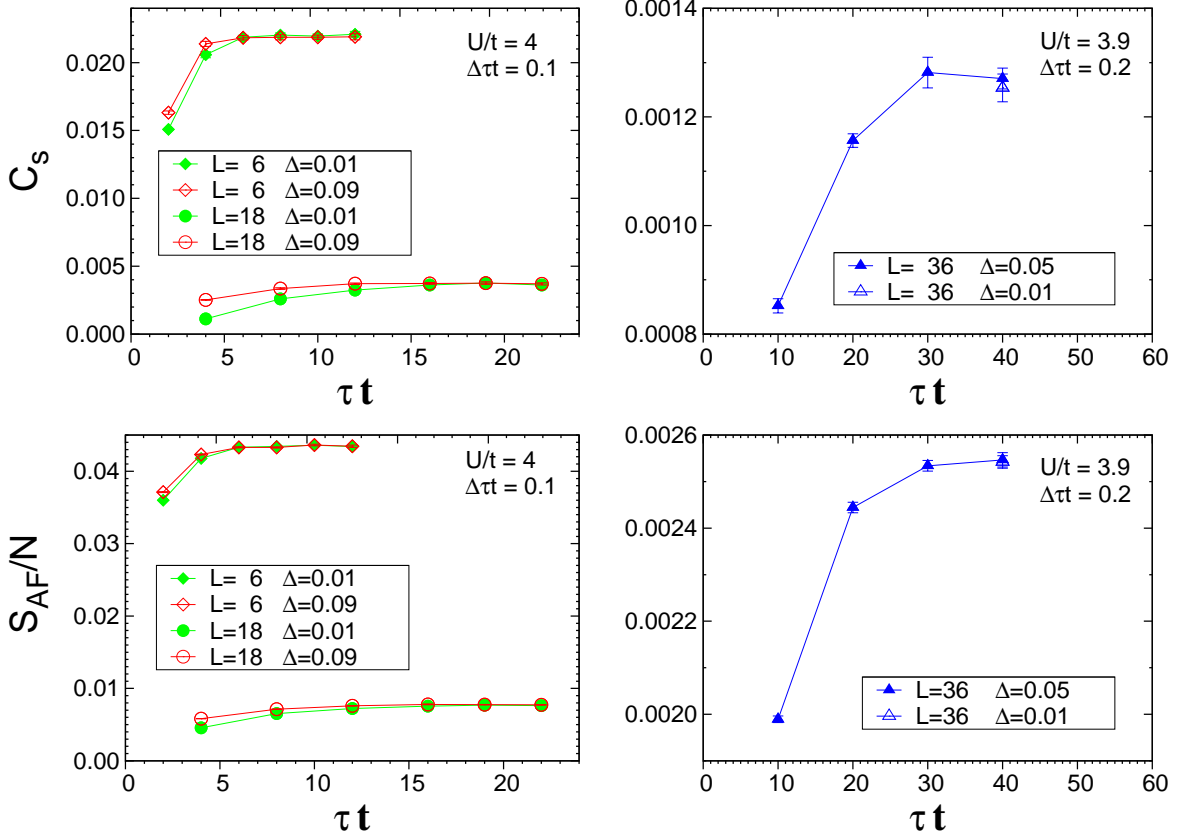


FIG. 7: The spin-spin correlations at the maximum distance  $C_s(L_{\max})$  (upper panels) and magnetic structure factor  $S_{AF}/N$  (lower panels) as a function of the projection time  $\tau$  for  $L = 6, 18$ , and  $L = 36$ .  $U/t$ ,  $\Delta\tau t$ , and  $\Delta$  used are indicated in the figures. The converged results are obtained at  $\tau t = L + 4$ , regardless of the chosen value of the parameter  $\Delta$  defining the left trial function  $|\psi_L\rangle$  in Eq. (20). Notice that, for  $\Delta$  larger than 0.01, the convergence to the ground state values ( $\tau \rightarrow \infty$ ) is apparently faster. The Gutzwiller parameter  $g$  in  $|\psi_L\rangle$  is set to be 0.72 for  $U/t = 4$  and  $L = 6, 18$ , and 0.65 for  $U/t = 3.9$  and  $L = 36$ . Notice also that these antiferromagnetic correlation functions,  $C_s(L_{\max})$  and  $S_{AF}/N$ , always monotonically increase within statistical errors with the projection time  $\tau$ , and converge even in the most difficult cases (right panels), namely, for the largest size very close to the critical  $U$  ( $U_c/t \sim 3.87$ ) below which the antiferromagnetic order disappears.

the ones reported in TABLES I–VIII can be considered to be accurate lower bounds of the order parameter.

Finally, the spin gap  $\Delta_s$  is estimated by directly calculating the ground state energies for the spin singlet sector [ $E(S = 0)$ ] and for the spin triplet sector [ $E(S = 1)$ ] separately, i.e.,

$$\Delta_s = E(S = 1) - E(S = 0). \quad (24)$$

The results are shown in TABLE IX calculated for various system sizes with  $L$  up to 18 and for different values of  $U/t$ . The thermodynamically extrapolated values for  $L \rightarrow \infty$  are estimated by fitting the results for different  $L$ 's with quadratic polynomials in  $1/L$  and these results are also shown in the last row of TABLE IX.

- 
- [1] B. Bernu, P. Lecheminant, C. Lhuillier, and L. Pierre, Phys. Rev. B **50**, 10048(1994).  
 [2] Z. Y. Meng, T. C. Lang, S. Wessel, F. F. Assaad, and A. Muramatsu, Nature **464**, 847 (2010).  
 [3] J. E. Hirsch, Phys. Rev. B **31**, 4403 (1985).  
 [4] H. F. Trotter, Proc. Amer. Math. Soc. **10**, 545 (1959); M.

- Suzuki, Commun. Math. Phys. **51**, 183 (1976).  
 [5] There is a misprint of a factor two in the plots of  $S_{AF}$  and  $C_s$  in Ref. 2 (A. Muramatsu *et al.*, private communication).

$L \backslash U/t$	3.7	3.8	3.9	4	4.1
6	0.01769(73)	0.018160(40)	0.019278(70)	0.02044(20)	0.021748(82)
9	0.007940(60)	0.008924(55)	0.00999(11)	0.01102(13)	0.012099(67)
12	0.004652(35)	0.005429(15)	0.006229(46)	0.007263(32)	0.008307(30)
15	0.003033(19)	0.003787(26)	0.00491(23)	0.005485(41)	0.006541(47)
18	0.002235(28)	0.002840(17)	0.003360(85)	0.004419(27)	0.005536(47)
24	0.001383(28)	0.001921(12)	0.002437(60)	0.003325(37)	0.004466(89)
36	0.000674(21)	0.0011659(73)	0.001658(82)	0.002380(67)	0.003487(49)
$\infty$ (i)	-0.00011(15)	0.000384(55)	0.00120(35)	0.00125(25)	0.00241(20)
$\infty$ (ii)	0.00048(39)	0.00076(19)	0.00155(65)	0.00148(43)	0.00332(56)
$\infty$ (iii)	-0.00018(20)	0.000264(95)	0.00098(56)	0.00102(38)	0.00184(35)

$L \backslash U/t$	4.2	4.3	4.4	4.5	4.6
6	0.023026(97)	0.02468(11)	0.025896(80)	0.027285(89)	0.02818(68)
9	0.013398(78)	0.014594(91)	0.01609(16)	0.01771(17)	0.01864(19)
12	0.009512(41)	0.01071(20)	0.012258(85)	0.01382(30)	0.01424(27)
15	0.007674(55)	0.00894(12)	0.01042(34)	0.01150(22)	0.0124(03)
18	0.006687(85)	0.00739(27)	0.00893(21)	0.01145(91)	0.0115(04)
24	0.00565(16)	0.00731(58)	0.00864(61)	0.0109(11)	0.0098(12)
36	0.00457(19)	0.00663(53)	—	0.00731(78)	—
$\infty$ (i)	0.00406(53)	0.0067(15)	—	0.0061(22)	—
$\infty$ (ii)	0.00510(84)	0.0051(28)	0.0057(23)	0.0141(53)	0.0120(49)
$\infty$ (iii)	0.00308(87)	0.0084(25)	—	0.0048(40)	—

TABLE I: Spin-spin correlations at the maximum distance  $C_s(L_{\max})$  for several values of  $U/t$ . Here  $\Delta\tau t = 0.4$  and projection time  $\tau t = L + 4$ . The extrapolated values for  $L \rightarrow \infty$  are obtained by cubic fits in  $1/L$  using (i) data corresponding to  $L = 6, 9, 12, 15, 18, 24, 36$ , (ii) data as in (i) but without the  $L = 36$  case (the largest size simulation), (iii) data as in (i) but without the  $L = 6$  case (the smallest size simulation). The corresponding error bars are computed with the resampling technique described in Methods of the main text. Notice that for  $U/t = 4.4$  and  $U/t = 4.6$  only (ii) is available as, in these cases, we have not performed the largest size simulation. The statistical errors are indicated by numbers in parentheses (corresponding to the last two digits).

$L \backslash U/t$	3.7	3.8	3.9	4	4.1
6	0.017641(50)	0.018946(98)	0.020350(77)	0.02147(13)	0.02332(13)
9	0.007859(40)	0.008868(28)	0.009878(54)	0.011107(44)	0.012434(86)
12	0.00473(21)	0.005204(15)	0.006078(24)	0.007090(90)	0.008227(39)
15	0.002868(22)	0.003515(14)	0.004215(31)	0.005249(70)	0.006239(32)
18	0.002043(18)	0.002571(17)	0.003210(28)	0.00404(04)	0.005011(27)
24	0.001133(13)	0.0015855(67)	0.002183(21)	0.002904(36)	0.003890(27)
36	0.000513(15)	0.0008547(53)	0.001271(19)	0.002014(72)	0.002943(31)
$\infty$ (i)	-0.000094(75)	0.000110(38)	0.000200(99)	0.00107(24)	0.00205(14)
$\infty$ (ii)	-0.00027(17)	0.00011(12)	0.00071(25)	0.00103(40)	0.00232(33)
$\infty$ (iii)	0.00000(17)	0.000067(63)	0.00005(17)	0.00115(48)	0.00199(24)

$L \backslash U/t$	4.2	4.3	4.4	4.5	4.6
6	0.02457(12)	0.02615(12)	0.02833(38)	0.03021(21)	0.03155(47)
9	0.013687(49)	0.015186(58)	0.01706(32)	0.0187(02)	0.02022(24)
12	0.009527(62)	0.010643(91)	0.012512(71)	0.014256(97)	0.0174(15)
15	0.00763(15)	0.00874(12)	0.01056(16)	0.01181(15)	0.01380(60)
18	0.006228(56)	0.00730(25)	0.00929(21)	0.01086(30)	0.0130(12)
24	0.00519(11)	0.00573(10)	0.00837(52)	0.00881(22)	0.01069(60)
36	0.00458(34)	0.00513(25)	—	0.00827(59)	—
$\infty$ (i)	0.00372(63)	0.00373(64)	—	0.0057(13)	—
$\infty$ (ii)	0.00336(73)	0.00286(81)	0.0083(27)	0.0046(15)	0.0038(55)
$\infty$ (iii)	0.0053(12)	0.0038(14)	—	0.0074(25)	—

TABLE II: Same as Table. I but for  $\Delta\tau t = 0.2$ .

$L \backslash U/t$	3.7	3.8	3.9	4	4.1
6	0.01783(14)	0.018970(50)	0.020525(69)	0.02234(29)	0.02371(19)
9	0.007859(20)	0.008791(19)	0.009842(30)	0.011013(33)	0.012464(72)
12	0.004381(43)	0.005117(12)	0.005978(25)	0.006930(40)	0.008094(34)
15	0.002796(18)	0.003446(20)	0.00412(03)	0.004999(52)	0.006109(41)
18	0.001959(42)	0.002474(23)	0.003091(23)	0.003869(26)	0.004945(59)
24	0.001096(11)	0.0015101(96)	0.002008(25)	0.002714(30)	0.003745(33)
36	0.0004969(50)	0.0007721(79)	0.001181(20)	0.001901(81)	0.002727(42)
$\infty$ (i)	0.000051(49)	0.000026(46)	0.000256(88)	0.00086(23)	0.00161(19)
$\infty$ (ii)	0.00010(16)	0.00015(12)	0.00024(22)	0.00066(32)	0.00213(38)
$\infty$ (iii)	0.00001(10)	-0.000089(78)	0.00027(17)	0.00105(40)	0.00108(30)

$L \backslash U/t$	4.2	4.3	4.4	4.5	4.6
6	0.025130(58)	0.02673(13)	0.02816(15)	0.03056(18)	0.03238(31)
9	0.013821(61)	0.015357(81)	0.017086(95)	0.01945(47)	0.02106(73)
12	0.00955(11)	0.01090(16)	0.012567(89)	0.01425(13)	0.01570(46)
15	0.007286(49)	0.00855(11)	0.01029(15)	0.01171(16)	0.0134(02)
18	0.005903(66)	0.00700(20)	0.00878(14)	0.01045(25)	0.0121(04)
24	0.004874(76)	0.00608(15)	0.00765(21)	0.00913(27)	0.01085(64)
36	0.00389(14)	0.00582(26)	—	0.0103(22)	—
$\infty$ (i)	0.00318(40)	0.00594(74)	—	0.0099(24)	—
$\infty$ (ii)	0.00319(58)	0.0046(11)	0.0054(13)	0.0095(23)	0.0116(43)
$\infty$ (iii)	0.00426(83)	0.0087(15)	—	0.0102(43)	—

TABLE III: Same as Table. I but for  $\Delta\tau = 0.1$ .

$L \backslash U/t$	3.7	3.8	3.9	4	4.1
6	0.01780(15)	0.019050(50)	0.020640(62)	0.02198(16)	0.02384(13)
9	0.007851(21)	0.008794(20)	0.009833(32)	0.011032(35)	0.012506(65)
12	0.004372(45)	0.005105(11)	0.005985(22)	0.006922(40)	0.008118(30)
15	0.002789(16)	0.003424(15)	0.004067(32)	0.005019(49)	0.006108(32)
18	0.001970(22)	0.002466(17)	0.003090(24)	0.003849(25)	0.004855(34)
24	0.001070(11)	0.0014780(74)	0.002022(22)	0.002699(27)	0.003697(30)
36	0.0004839(55)	0.0007488(57)	0.001147(21)	0.001879(66)	0.002719(32)
$\infty$ (i)	0.000050(48)	0.000002(36)	0.000143(92)	0.00099(20)	0.00173(14)
$\infty$ (ii)	-0.00008(15)	0.00001(11)	0.00033(21)	0.00085(28)	0.00203(32)
$\infty$ (iii)	0.00008(10)	-0.000061(61)	0.00012(16)	0.00106(36)	0.00150(24)

$L \backslash U/t$	4.2	4.3	4.4	4.5	4.6
6	0.025247(59)	0.02677(11)	0.02839(15)	0.03090(16)	0.03266(31)
9	0.013819(49)	0.015395(62)	0.01716(10)	0.01909(22)	0.02082(30)
12	0.009539(69)	0.01073(11)	0.012592(70)	0.01433(11)	0.01594(48)
15	0.007283(51)	0.008566(96)	0.01038(14)	0.01180(14)	0.01348(20)
18	0.005950(54)	0.00706(18)	0.00890(14)	0.01043(26)	0.01227(39)
24	0.004866(75)	0.00577(15)	0.00764(23)	0.00879(28)	0.01094(57)
36	0.00392(15)	0.00538(23)	—	0.00880(79)	—
$\infty$ (i)	0.00307(39)	0.00482(65)	—	0.0070(16)	—
$\infty$ (ii)	0.00291(55)	0.0034(10)	0.0054(12)	0.0056(18)	0.0104(36)
$\infty$ (iii)	0.00435(73)	0.0060(13)	—	0.0094(29)	—

TABLE IV: Same as Table. I, but  $\Delta\tau$  is extrapolated to 0 by fitting the  $\Delta\tau = 0.4, 0.2,$  and  $0.1$  data with quadratic polynomial in  $\Delta\tau$  for each  $L$ . The extrapolations for  $L \rightarrow \infty$  in (i), (ii), and (iii) are performed using the  $\Delta\tau \rightarrow 0$  extrapolated results for different  $L$ 's.

$L \backslash U/t$	3.7	3.8	3.9	4	4.1
6	0.035808(97)	0.037194(23)	0.038750(51)	0.04014(11)	0.041717(46)
9	0.017779(18)	0.018998(19)	0.020288(50)	0.021568(17)	0.0230043(91)
12	0.010880(24)	0.0118617(61)	0.012927(21)	0.014172(13)	0.015485(15)
15	0.007430(17)	0.008309(11)	0.009333(65)	0.010380(16)	0.011678(26)
18	0.005495(18)	0.006260(12)	0.006932(41)	0.008199(12)	0.009405(14)
24	0.003368(11)	0.0040547(51)	0.004737(21)	0.005831(17)	0.007026(12)
36	0.0017280(89)	0.0023083(29)	0.002911(38)	0.003909(37)	0.005001(20)
$\infty$ (i)	-0.000260(50)	0.000200(24)	0.00078(16)	0.00142(11)	0.002433(68)
$\infty$ (ii)	-0.00046(14)	0.000121(82)	0.00070(27)	0.00137(15)	0.00259(12)
$\infty$ (iii)	-0.000156(99)	0.000207(39)	0.00099(25)	0.00161(17)	0.00239(12)

$L \backslash U/t$	4.2	4.3	4.4	4.5	4.6
6	0.043429(70)	0.045119(28)	0.046740(33)	0.048433(35)	0.05051(61)
9	0.024512(28)	0.026082(49)	0.027721(49)	0.029377(37)	0.030936(71)
12	0.016901(23)	0.018318(75)	0.020054(39)	0.021689(46)	0.022623(73)
15	0.012990(21)	0.014471(49)	0.016051(47)	0.01778(12)	0.01907(09)
18	0.010766(37)	0.01202(10)	0.01404(24)	0.01519(19)	0.0170(02)
24	0.008317(43)	0.009578(66)	0.01114(12)	0.01255(11)	0.01424(44)
36	0.006268(77)	0.00781(25)	—	0.01014(28)	—
$\infty$ (i)	0.00375(20)	0.00487(47)	—	0.00630(54)	—
$\infty$ (ii)	0.00387(28)	0.00458(51)	0.00579(67)	0.00630(64)	0.0156(18)
$\infty$ (iii)	0.00382(36)	0.0052(11)	—	0.0061(14)	—

TABLE V: Spin structure factors  $S_{\text{AF}}/N$  for several values of  $U/t$ . Here  $\Delta\tau t = 0.4$  and projection time  $\tau t = L + 4$ . The extrapolated values for  $L \rightarrow \infty$  are obtained by cubic fits in  $1/L$  using (i) data corresponding to  $L = 6, 9, 12, 15, 18, 24, 36$ , (ii) data as in (i) but without the  $L = 36$  case (the largest size simulation), (iii) data as in (i) but without the  $L = 6$  case (the smallest size simulation). The corresponding error bars are computed with the resampling technique described in Methods of the main text. Notice that for  $U/t = 4.4$  and  $U/t = 4.6$  only (ii) is available as, in these cases, we have not performed the largest size simulation. The statistical errors are indicated by numbers in parentheses (corresponding to the last two digits).

$L \backslash U/t$	3.7	3.8	3.9	4	4.1
6	0.037612(28)	0.039255(45)	0.041014(29)	0.042784(74)	0.044697(46)
9	0.018340(20)	0.019643(14)	0.020993(15)	0.022476(18)	0.024054(16)
12	0.011030(23)	0.0120164(68)	0.013139(13)	0.014402(18)	0.015865(15)
15	0.007408(14)	0.0082476(90)	0.009205(13)	0.010359(18)	0.0116936(87)
18	0.0053791(90)	0.0060880(99)	0.006924(14)	0.00799(02)	0.009248(13)
24	0.0031972(77)	0.0037857(29)	0.004508(11)	0.005467(20)	0.006654(10)
36	0.0015324(71)	0.0019833(29)	0.002547(15)	0.003375(23)	0.004500(13)
$\infty$ (i)	-0.000373(36)	-0.000092(19)	0.000152(58)	0.000761(83)	0.001724(51)
$\infty$ (ii)	-0.000570(95)	-0.000157(64)	0.00018(11)	0.00089(17)	0.001736(97)
$\infty$ (iii)	-0.000268(76)	-0.000085(30)	0.00016(10)	0.00065(15)	0.001810(97)

$L \backslash U/t$	4.2	4.3	4.4	4.5	4.6
6	0.046595(44)	0.048480(74)	0.05085(15)	0.052760(89)	0.05521(25)
9	0.025775(18)	0.027578(22)	0.029571(60)	0.03158(05)	0.033680(99)
12	0.017409(16)	0.019056(51)	0.021001(26)	0.022981(59)	0.024851(98)
15	0.013224(25)	0.014875(60)	0.016683(49)	0.018522(42)	0.02037(18)
18	0.010672(17)	0.01222(16)	0.014087(51)	0.015852(79)	0.01789(30)
24	0.008040(49)	0.009472(36)	0.011225(81)	0.013113(90)	0.01525(25)
36	0.005907(41)	0.00735(12)	—	0.01092(23)	—
$\infty$ (i)	0.00319(13)	0.00432(30)	—	0.00781(48)	—
$\infty$ (ii)	0.00293(25)	0.00407(36)	0.00556(52)	0.00759(58)	0.0114(14)
$\infty$ (iii)	0.00336(21)	0.00436(68)	—	0.00874(95)	—

TABLE VI: Same as Table. V but for  $\Delta\tau t = 0.2$ .

$L \backslash U/t$	3.7	3.8	3.9	4	4.1
6	0.038120(65)	0.039777(32)	0.041607(45)	0.043467(73)	0.045326(52)
9	0.018478(12)	0.0197460(90)	0.021142(16)	0.022633(14)	0.024266(15)
12	0.010999(14)	0.0120133(85)	0.013127(11)	0.014399(15)	0.015846(15)
15	0.007357(12)	0.0082117(80)	0.00914(01)	0.010291(18)	0.0116167(90)
18	0.005295(11)	0.0060164(83)	0.006851(12)	0.007875(18)	0.009134(17)
24	0.0031298(50)	0.0037011(36)	0.0043775(59)	0.005280(11)	0.0064862(86)
36	0.0015024(20)	0.0018748(44)	0.0024468(99)	0.003225(28)	0.004250(23)
$\infty$ (i)	-0.000166(22)	-0.000260(22)	0.000136(44)	0.000568(86)	0.001478(69)
$\infty$ (ii)	-0.000349(81)	-0.000293(54)	0.000004(85)	0.00045(12)	0.001626(91)
$\infty$ (iii)	-0.000104(44)	-0.000258(38)	0.000182(71)	0.00063(16)	0.00121(13)

$L \backslash U/t$	4.2	4.3	4.4	4.5	4.6
6	0.047429(27)	0.049415(49)	0.051481(68)	0.05401(24)	0.05610(12)
9	0.026021(30)	0.027858(19)	0.029900(36)	0.031952(33)	0.03438(27)
12	0.017458(35)	0.019281(89)	0.021168(35)	0.023206(63)	0.02508(17)
15	0.013083(30)	0.014722(39)	0.016661(89)	0.018642(67)	0.02070(08)
18	0.010558(32)	0.01212(11)	0.014063(72)	0.015833(76)	0.0179(01)
24	0.007796(26)	0.009361(42)	0.01113(12)	0.01314(23)	0.01498(15)
36	0.005492(66)	0.00752(13)	—	0.01022(22)	—
$\infty$ (i)	0.00252(18)	0.00466(31)	—	0.00609(60)	—
$\infty$ (ii)	0.00260(24)	0.00413(37)	0.00534(60)	0.0060(10)	0.0094(13)
$\infty$ (iii)	0.00246(36)	0.00685(78)	—	0.0068(10)	—

TABLE VII: Same as Table. V but for  $\Delta\tau = 0.1$ .

$L \backslash U/t$	3.7	3.8	3.9	4	4.1
6	0.038233(42)	0.039947(30)	0.041782(33)	0.043679(65)	0.045621(43)
9	0.018525(12)	0.0198080(89)	0.021207(16)	0.022723(13)	0.024369(13)
12	0.011020(14)	0.0120453(66)	0.013158(10)	0.014433(14)	0.015918(13)
15	0.007368(11)	0.0082122(73)	0.009129(13)	0.010311(15)	0.0116376(86)
18	0.0053070(91)	0.0060089(77)	0.006863(12)	0.007879(15)	0.009158(13)
24	0.0031187(50)	0.0036857(29)	0.0043622(63)	0.005259(11)	0.0064725(80)
36	0.0014867(23)	0.0018627(31)	0.002417(10)	0.003187(23)	0.004282(15)
$\infty$ (i)	-0.000206(21)	-0.000239(18)	0.000075(45)	0.000497(74)	0.001493(53)
$\infty$ (ii)	-0.000449(72)	-0.000315(49)	-0.000035(85)	0.00036(11)	0.001506(82)
$\infty$ (iii)	-0.000121(44)	-0.000207(30)	0.000105(74)	0.00051(13)	0.001494(99)

$L \backslash U/t$	4.2	4.3	4.4	4.5	4.6
6	0.047688(28)	0.049679(47)	0.051846(68)	0.05424(11)	0.05649(14)
9	0.026167(21)	0.028002(18)	0.030071(36)	0.032170(31)	0.03460(12)
12	0.017556(20)	0.019318(59)	0.021280(27)	0.023350(53)	0.02547(11)
15	0.013186(24)	0.014794(38)	0.016830(56)	0.018737(52)	0.020809(84)
18	0.010605(21)	0.01216(10)	0.014077(69)	0.015934(72)	0.01800(15)
24	0.007789(26)	0.009384(35)	0.011197(88)	0.01328(11)	0.01511(16)
36	0.005642(47)	0.00738(12)	—	0.01057(20)	—
$\infty$ (i)	0.00262(14)	0.00442(27)	—	0.00716(47)	—
$\infty$ (ii)	0.00225(20)	0.00404(32)	0.00525(48)	0.00733(65)	0.0098(11)
$\infty$ (iii)	0.00295(24)	0.00588(64)	—	0.00806(87)	—

TABLE VIII: Same as Table. V, but  $\Delta\tau$  is extrapolated to 0 by fitting the  $\Delta\tau = 0.4, 0.2,$  and  $0.1$  data with quadratic polynomial in  $\Delta\tau$  for each  $L$ . The extrapolations for  $L \rightarrow \infty$  in (i), (ii), and (iii) are performed using the  $\Delta\tau \rightarrow 0$  extrapolated results for different  $L$ 's.

$L \backslash U/t$	3.4	3.7	4	4.3
6	0.11452(62)	0.13034(48)	0.14054(68)	0.14287(94)
9	0.0828(11)	0.09672(72)	0.1032(10)	0.1020(22)
12	0.06292(97)	0.07611(99)	0.08212(92)	0.0753(24)
15	0.0524(11)	0.0634(12)	0.06743(92)	0.0616(26)
18	—	—	0.0558(10)	—
$\infty$	-0.0009(71)	0.0021(61)	-0.0018(42)	-0.013(16)

TABLE IX: The spin gap  $\Delta_S = E(S = 1) - E(S = 0)$  for several values of  $U/t$ . Here we set  $\Delta\tau t = 0.14$  and projection time  $\tau t = L + 4$ . The extrapolated values for  $L \rightarrow \infty$  are obtained by a quadratic fit in  $1/L$  and the corresponding error bars are computed with the resampling technique described in Methods of the main text. The statistical errors are indicated by numbers in parentheses (corresponding to the last two digits).